

# Non-linear Hysteresis Compensation of a Tendon-sheath-driven Robotic Manipulator using Motor Current

Dong-Ho Lee<sup>1</sup>, Young-Ho Kim<sup>2</sup>, Jarrod Collins<sup>2</sup>, Ankur Kapoor<sup>2</sup>, Dong-Soo Kwon<sup>1</sup>, and Tommaso Mansi<sup>2</sup>

**Abstract**—Tendon-sheath-driven manipulators (TSM) are widely used in minimally invasive surgical systems due to their long, thin shape, flexibility, and compliance making them easily steerable in narrow or tortuous environments. Many commercial TSM-based medical devices have non-linear phenomena resulting from their composition such as backlash and dead zone hysteresis, which lead to a considerable challenge for achieving precise control of the end effector pose. However, many recent works in the literature do not consider the combined effects and compensation of these phenomena, and less focus on practical ways to identify model parameters in real field. In this paper, we propose a simplified piece-wise linear model to compensate both backlash and dead zone hysteresis together. Further, we introduce a practical method to identify model parameters using motor current from a robotic controller for the TSM. We analyze our proposed methods with multiple Intra-cardiac Echocardiography catheters, which are typical commercial example of TSM. Our results show that the errors from backlash and dead zone hysteresis are considerably reduced and therefore the accuracy of robotic control is improved when applying the presented methods.

## I. INTRODUCTION

The tendon-sheath mechanism (TSM) is a popular control method that has been applied in many therapeutic [1, 2, 3, 4, 5] and real-time diagnostic (*e.g.* endoscope [6, 7, 8, 9], colonoscope [10], and Intra-cardiac Echocardiography [11, 12]) manipulators to achieve steerability by providing a long, thin, flexible structure that is compliant with anatomy. These TSM-based steerable manipulators are favorable in narrow and tortuous conditions, which makes them well-situated in relation to the growing shift towards minimally invasive treatment.

While the TSM-based manipulator has many advantages and wide adoption, the performance is still limited by non-linear frictional behaviors caused by: 1) backlash hysteresis due to friction forces between the sheath and tendons, 2) dead zone due to structural wire slack in the driving parts, and 3) plastic torsion due to the complex arrangement of threads and tubes about the center of the device. These factors contribute to the degradation of control accuracy and limit the potential performance of robotic controllers for off-the-shelf TSM-based devices.

Simple TSM-based applications consist of a polymer sheath with one to four sliding thread tendons equally spaced concentrically within the sheath. Many common commercial products (*e.g.* endoscopy, Intra-cardiac Echocardiography (ICE), Transesophageal Echocardiography (TEE), etc.) utilize two

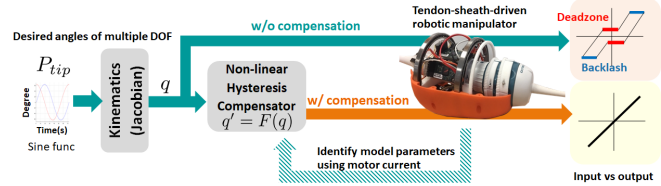


Fig. 1. A representative diagram and scenario: Given desired pose at a given time, our goal is to compensate the configuration states, finding a compensated motions that minimizes errors. The compensated configuration  $q'$  gives input equal to output while  $q$  without compensation generates dead zone and backlash. A novel ideas are that 1) we propose a simplified hysteresis model for both dead zone and backlash. 2) the model parameters are mainly identified using motor current with behavior motions.

antagonistic pairs of tendons which are each bound to control knobs at the proximal end of the device. An individual tendon can then be pulled, and the distal tip of the device bent, by rotating the associated control knob; thus, allowing the antagonistic tendon to remain inactive. This structure assumes an ideal zero-slack transition between paired tendons; however, this is not realistically achievable. Moreover, the center of the device can either be hollow or house multiple components in a central channel (*e.g.* camera, ultrasound transducer, grasping tools). Highly non-linear behaviors exist because of these structural considerations.

Accordingly, flexible TSM manipulators for different tasks will have different non-linear hysteresis of the tendon threads. An external robotic control system would therefore need to calibrate these effects before accurate manipulation can be achieved. Whether robotic control is being considered for disposable or reusable TSM manipulators, calibration would be required before each use.

Precise prediction of the tool tip pose for a specific knob configuration is challenged by these non-linear properties. Moreover, there are practical limitations (*i.e.* sterilization, cost, and size) which restrict adding traditional sensors to the tool tip to provide the necessary feedback for closed-loop control. As such, the control strategy for such a robotic system is open loop with no spatial feedback. However, much research has focused on modeling TSM itself without consideration of practical constraints and needs.

In this paper, we introduce new methods to model non-linear hysteresis and a practical method for calibration of application in robotic control for TSM manipulators. More specifically, (1) we propose a simplified piece-wise linear model to compensate non-linear hysteresis of both backlash and dead zone together and (2) in response to limitations in current practical settings, we validate the relationship between non-linear hysteresis and motor current experimentally. Then, we propose a parameter identification method which associates motor current to

<sup>1</sup>Korea Advanced Institute of Science and Technology, Daejeon, South Korea vanquisher90@gmail.com, kwonds@kaist.ac.kr

<sup>2</sup>Siemens Healthineers, Digital Technology & Innovation, Princeton, NJ, USA {young-ho.kim, jarrod.collins, ankur.kapoor, tommaso.mansi}@siemens-healthineers.com

particular motion behavior. Finally, we evaluate the proposed methods on benchtop with multiple catheters.

## II. RELATED WORK

Recently, several researchers have addressed the non-linear characteristics of TSM with various analytical models (*e.g.*, friction, hysteresis models), image-based and data-driven approaches.

To overcome backlash hysteresis, many studies have proposed a static model using coulomb friction [13, 14, 15, 16, 17, 18, 19]. Tension propagation is represented with a friction coefficient and the radius curvature (the shape) of the sheath. However, it could not reflect the dynamic effect when the direction was changed, and the backlash function is discontinuous.

Various mathematical models including differential equations such as Bouc-Wen model and Prandtl-Ishlinskii model have also been proposed to reflect the dynamic characteristics [20, 21, 22, 23]. However, there exist many hyperparameters, and the parameter identification is complicated. Mostly, additional sensors are required with controlled environments. In addition, they focus on varied shapes of backlash hysteresis rather than considering dead zone. The enhanced Bouc-Wen model considers the dead zone like shape (called as pinching [24]), however their main module (*i.e.* energy function) is for structural engineering application (vibration, stress modeling), which is not relevant to continuously manipulating system.

Image-based method is also proposed [25, 26, 27]. This method is more robust than the previous methods in which the model's performance is affected when the shape of the sheath changes. Pose of the bending section is estimated through the obtained image, and feedback compensation is performed using the difference between the predicted bending angle and the input bending angle. However, the performance may change depending on the image quality or the presence of obstacles.

In order to overcome the dead zone, a data-driven method has been proposed [28, 29]. Data is obtained by sweeping the bending section up/down and left/right before use, and the motion was compensated by mapping the input and output data. However, this method also always required an additional sensor before use.

Although various attempts have been made, additional sensors such as load cells, vision sensors, and encoders were required, and it is hard to attach additional sensors in a clinical environment. Also, only one degree of freedom is considered, and no studies have considered both backlash hysteresis and dead zone together.

## III. MATERIALS AND METHODS

### A. Tendon-sheath-driven robotic manipulator

An overview of the robotic system is illustrated in Figure 1. This is a typical open-loop control diagram for tendon-sheath-driven robotic manipulators. Herein, we focus on how to model



Fig. 2. (a)-(b) Illustrative examples of 2-DOF TSM-based manipulators: ACUSON AcuNav Volume ICE catheter, ACUSON V5Ms TEE probe. Source: Siemens Healthineers. (c) 2-DOF TSM-based body cross-section: four thread sections (orange) combining with polymer cover (black) and ultrasound array (green)

and identify hysteresis compensation. Therefore, we do not revisit fundamental forward and inverse kinematics in this paper. The detailed kinematics models can be found in [30, 11, 12].

We briefly review our motorized system that can manipulate multiple degree-of-freedom (DOF) tendon-sheath-driven devices. The robot has four degrees of freedom; two DOFs for steering the tip in two planes (anterior-posterior knob angle  $\phi_1$  and right-left knob angle  $\phi_2$ ) using two knobs on the handle, and other two DOFs for bulk rotation and translation along the major axis of the catheter body. Since rotation and translation do not contribute to the hysteresis phenomenon, we will focus on the two knob controls. We define the robot's configuration state,  $\mathbf{q} = (\phi_1, \phi_2)$  in  $\mathbb{R}^2$ .

Figure 1 also shows an exemplary scenario. First, the desired pose of the tip  $P_{tip}$  is given. Second, the desired robotic configuration state  $\mathbf{q}$  is computed from the inverse kinematics model. Next, our compensator  $F$  is applied to compute the compensated motor configuration  $\mathbf{q}'$ , which is directly applied to the motors. Then, the input versus the real output curve ideally shows a diagonal line for  $\mathbf{q}'$  (*i.e.* when properly compensated) while  $\mathbf{q}$  (*i.e.* without compensation) might show a hysteresis curve including deadzone and backlash.

Since external sensors (*e.g.* load cell, electromagnetic (EM) tracker) are not considered in the field, we believe the only input that we can use is motor current relative to enacted motions. Thus, we analyze a relationship between the motor current and hysteresis curve in Section III-B.

### B. Systematic analysis of motor current and hysteresis curve

In order to find out the relationship between the non-linear hysteresis and the motor current, we conduct a systematic test where the desired input is a simple sweep motion in the form of a sine wave that has been commonly used in other studies [18, 19, 21, 22, 23, 31, 32, 27]. The sweeping angle range is  $\pm 90^\circ$ , and collected data for  $\phi_1$  and  $\phi_2$ . Two cycles of sweeping motions are applied with  $40^\circ/\text{sec}$ , and the shape of the sheath is constrained to remain straight.

We collect the following data with the sine wave motion for each knob: (1) the desired robot configuration input ( $\phi_1, \phi_2$ ), (2) the real output angle of the bending section using EM tracker (3D guidance, Northern Digital Inc.), ( $\phi_1^{EM}, \phi_2^{EM}$ ), and (3) the motor current  $c$  acquired from motor drivers in real time. We applied the proper filter for all settings (3rd order Butterworth filter, cutoff frequency 20 hz). We demonstrate one representative data to understand the relationship between hysteresis curve and motor current. Figure 3(a) shows the

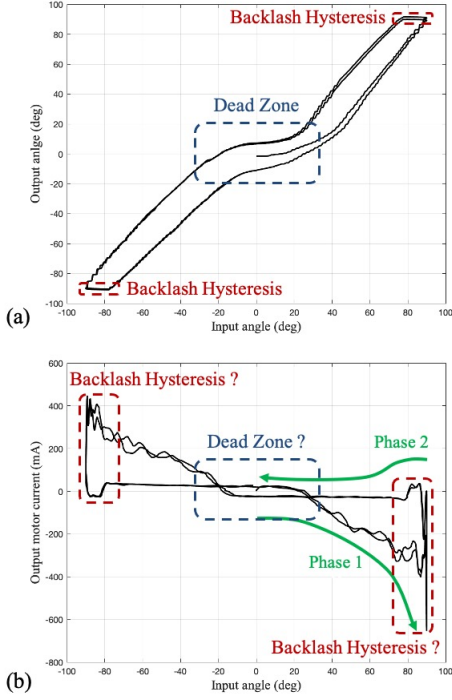


Fig. 3. One analytical data represents dead zone and backlash hysteresis: (a) the desired robot state  $\phi_1$  versus the real output angle  $\phi_1^{EM}$  (b) the desired robot state  $\phi_1$  versus the motor current.

desired angle versus the real output angle. Figure 3(b) shows the desired angle versus the real output current.

**Lesson 1** from Figure 3(a): We know the desired input and the real output should be the same if for an ideal TSM. However, this shows multiple non-linear behaviors: (1) *dead zone* when the input angle is near zero, there is a dead zone that maintains a constant output value even if the input value increases (or decreases). (2) *backlash hysteresis* when the direction of motion is changed, there is delay in the real output angle rather than immediately increasing (or decreasing) the angle.

**Lesson 2** from Figure 3(b): To explain the motor current behaviors, we classify two phases; (1) *phase 1 (dead zone)*: This is an interval from  $0^\circ$  to  $90^\circ$ . As the input is increased from  $0^\circ$  to a certain angle, there exist a smooth flat signal shape. Also the current magnitude remains a constant value in this section. However, when exceeding the certain angle, the output angle is gradually increased, and the current magnitude is increased according to the output angle. The same phenomenon is observed when moving in the opposite direction. Thus, we believe that the current measure can be used to detect the dead zone width. (2) *phase 2 (backlash)*: This is an interval from  $90^\circ$  to  $0^\circ$ . The moment that the desired input changes direction shows an interesting phenomenon such that the output angle is maintained for some time before it is gradually decreased. Looking at the behavior of the motor current at this time, the current direction changes sharply in the opposite direction, and after making a small peak, it was kept constant at a value near zero. The reason for the peak is that when the wire changes from pulling to releasing, the tension does not change

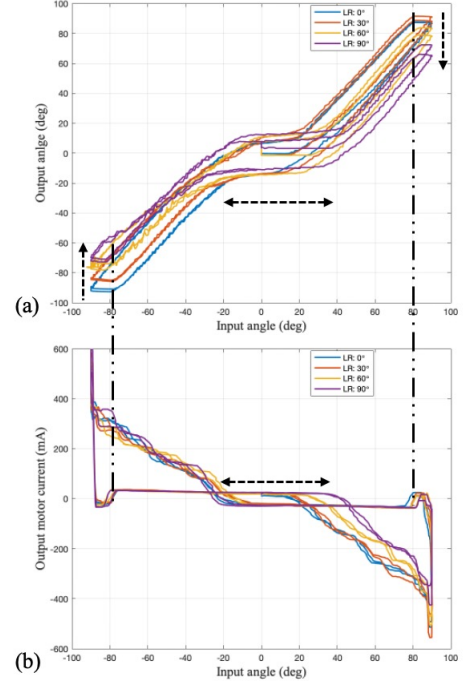


Fig. 4. Sweeping motion for  $\phi_1$  when  $\phi_2$  is varied positively (equal to 0, 30, 60; (a) hysteresis curve of (b) motor current of  $\phi_1$

immediately, but because there is a transitional phase in which the tension gradually decreases, finally it will stay a certain current level as tension is balanced. We can observe that the point at which the current begins to become constant and the point at which the backlash hysteresis ends are related. Thus, we believe the critical points of backlash and dead zone can be represented by motor current measures.

**Lesson 3** from Figure 4: Additionally, we check whether one DOF affects other DOF.  $\phi_1$  is swept while  $\phi_2$  is constant. We varied  $\phi_2$  from  $0^\circ$  to  $90^\circ$  with  $30^\circ$  intervals. Figure 4(a) shows the dead zone is shifted as the fixed value of  $\phi_2$  is increased. The same phenomenon is occurred with the motor current in Figure 4(b). In the case of the backlash hysteresis, there is no significant change in either graph. However, we observe that the backlash hysteresis ends and the motor current remains constant after the small peak is observed. Furthermore, in Fig. 4(a), the slopes of the output were similar except for the dead zone and backlash period, and also the output angles in the dead zone were similar. The opposite direction, *i.e.* when  $\phi_2$  is decreased from  $0^\circ$  to  $-90^\circ$ , is not shown here, but the result is symmetric, which is biased to the negative side.

#### C. Modeling non-linear hysteresis using piecewise linear approximation

As shown in Figure 4(a), we have a highly non-linear object curve, but our given input is desired input and motor current. Therefore, we propose a piecewise linear approximation to represent the non-linear hysteresis phenomenon. Our model consists of a total of eight line equations, half of which are when the velocity is positive and others are when the velocity is negative. To define a finite collection of linear functions,

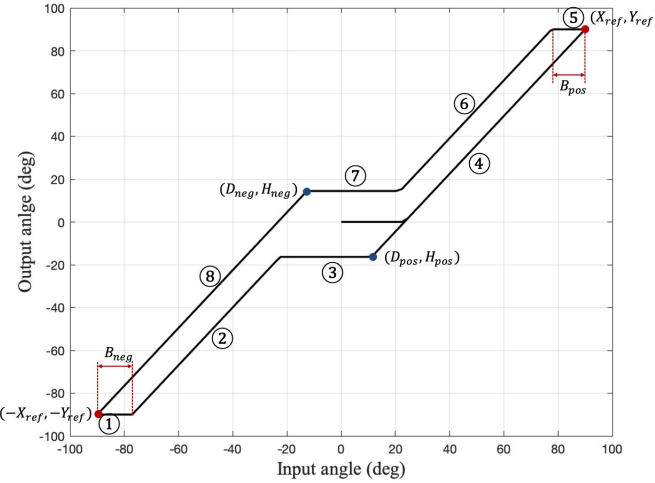


Fig. 5. Our proposed piecewise linear model: eight equations represent nonlinear hysteresis phenomena.

we define four parameters; the range of the dead zone ( $D$ ), the height of the dead zone ( $H$ ), the size of the backlash hysteresis ( $B$ ), and the slope of the lines ( $A$ ) when the velocity is positive and negative, respectively. All parameters of our proposed method are shown in Figure 5. Additionally, we define  $(X_{ref}, Y_{ref})$  as a reference point, which is the degree of the input and the degree of the real output, respectively, and we made following three design decisions to reduce the complexity of the model.

**Design Decision 1:** We assume that  $X_{ref}$  and  $Y_{ref}$  are given when one DOF is swept while another DOF is fixed to 0 degree.

**Rationale:** This is a reasonable assumption since another DOF stays on 0 degree, so we can minimize interference while one DOF is swept. The commercial catheter is usually calibrated for  $\phi_1$  and  $\phi_2$  with regard to real output for reference axis like  $\pm 90^\circ$ . In this manner, it becomes fairly trivial to acquire a reference point in specific condition (*i.e.*,  $(\phi_1, \phi_2) = \{(0, 90), (90, 0), (-90, 0), \dots\}$ ) by visual inspection.

**Design Decision 2:** The slope of the lines  $A$  of the one target device is constant.

**Design Decision 3:** The height of the dead zone  $H$  is constant for the target device.

**Rationale:** As our target device is a commercial product, so its physical properties are optimized as similar. We bring this data from mechanical data sheets, or we simply can measure it one time for each product.

Accordingly, we define eight linear equations composed of four parameters and given assumptions. Figure 5 shows how the equations are divided over the region and each equation is addressed in Equations(1) to (8).

$$\text{Line 1: } y = A(-X_{ref} - D_{neg}) + H_{neg} \quad (1)$$

$$\text{Line 2: } y = A(x - D_{neg} - B_{neg}) + H_{neg} \quad (2)$$

$$\text{Line 3: } y = H_{pos} \quad (3)$$

$$\text{Line 4: } y = A(x - D_{pos}) + H_{pos} \quad (4)$$

$$\text{Line 5: } y = A(X_{ref} - D_{pos}) + H_{pos} \quad (5)$$

$$\text{Line 6: } y = A(x - D_{pos} + B_{pos}) + H_{pos} \quad (6)$$

$$\text{Line 7: } y = H_{neg} \quad (7)$$

$$\text{Line 8: } y = A(x - D_{neg}) + H_{neg} \quad (8)$$

The dead zone (3, 7) and backlash hysteresis (1, 5) parts consist of a line with the slope of zero, and the other parts consist of a line with the slope of  $A$ . When the velocity is positive, the output moves on lines 2, 3, and 4 located at the bottom, and when the velocity is negative, the output moves on lines 6, 7, and 8 located at the top. When the direction of movement changes, the output moves on lines 1, and 5 that can give the backlash hysteresis effect.

#### D. Parameter Identification

In order to use our proposed model, we need to identify the model parameters along with target devices. Based on above lessons, we use motor current to identify four parameters with given the reference point  $(X_{ref}, Y_{ref})$ .

**1) One DOF calibration procedure:** We start to explain one DOF calibration method assuming other DOFs zero. The range of the dead zone ( $D_{pos}, D_{neg}$ ) and the size of the backlash hysteresis ( $B_{pos}, B_{neg}$ ) were measured through the motor current. The dead zone is obtained by selecting a moment when the period of constant current ends and it starts to increase or decrease. To find this moment, the 'findchangepts' function in Matlab was used. This function returns the index at which the mean value changes the most in the data, so the moment when the slope changes sharply can be found. The size of the backlash hysteresis is obtained by selecting the moment at which the current starts to become constant after a small peak after changing the moving direction. To find this moment, the 'findpeak' function in Matlab was used. This function finds the local maxima in the data, and the local minima can be obtained by multiplying the data by -1 and using this function.

The slope of the line ( $A$ ), which is not obtained from the motor current, however we can compute this from  $D$  and given  $(X_{ref}, Y_{ref})$  and  $H$  (see design decision 1-3). Now we have  $B$  and  $D$  from motor current, and  $A$  with given  $(X_{ref}, Y_{ref})$  and  $H$ . Thus, we can identify all parameters of one DOF hysteresis function  $F$ .

The slope of the line ( $A$ ), which is not obtained from the motor current, however we could get 'A' using collected data for four ICE catheters. From there, we got the average value 1.32 and the standard deviation is 0.12, indicating that most of them had similar slopes. Lastly, the height of the dead zone ( $H_{pos}, H_{neg}$ ) were calculated using the parameters obtained earlier. The slope of the line is already determined, and it must be the same as the slope of the line passing the reference point

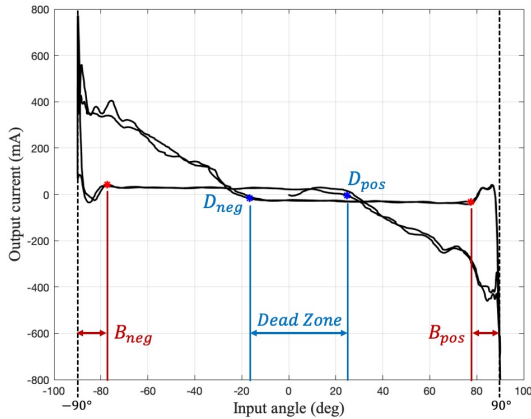


Fig. 6. Identification of the size of the backlash hysteresis and the range of the dead zone in the motor current data

and the point where the dead zone ends, so the height of the dead zone can be calculated. The values obtained are used continuously in one catheter (see design decision 1-3).

2) *Multiple DOF calibration procedure*: For multiple DOF calibration, we collect the motor current with systematic motion behaviors; First, one DOF is sweeping  $\pm 90$ , while other DOFs are fixed at certain conditions. (We changed other DOFs  $0, \pm 30, \pm 60, \pm 90$  degrees.) Second, we can extract the range of deadzone  $D$  and the size of backlash  $B$  from motor current using change of points algorithms. Third, We can get  $D$  changed depending on other DOFs conditions. However, we have  $A$  and  $H$  from one DOF calibration procedure in Section III-D1. So given  $A$ ,  $H$ , and  $D$ , we can compute the reference point differently for each condition.

Due to the limited resources, we could not apply all possible motion combinations with multiple DOFs calibration. From discrete motion combination ( $\pm 90^\circ$  at  $30^\circ$  intervals), we can interpolate  $D$  based on collected data. We show one real data as a example in Figure 7.  $D_{pos}$  shows a downward convex bell shape, and  $D_{neg}$  shows an upward convex bell shape. Accordingly, we can estimate all conditions of parameters. Then, the model calibration is completed for the whole workspace.

Now we have compensator  $F$ , which covers the whole workspace for multiple DOF TSM manipulator. This compensation is used as a feed-forward control after receiving the desired input. Then, the desired input  $\mathbf{q}$  can be compensated by  $\mathbf{q}'$  as shown Figure 1.

#### IV. EXPERIMENT AND RESULT

##### A. Experimental Setup

We used ICE catheter with robotic system shown in Figure 1, and Figure 2(a). The ICE catheter consists of two knobs, which controls  $\phi_1$  and  $\phi_2$ . First, we carried on parameter identification using methods in Section III-D. As mentioned in Section III-D1, we used ' $A$ ' as 1.32 as the average value, then  $H$  is computed with the determined parameters.

Then, we conducted two experiments; (1) *One DOF test*: One DOF knob is swept  $\pm 60$  while another DOF is a constant,

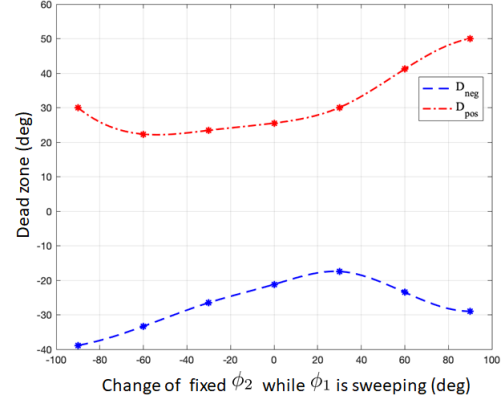


Fig. 7. anterio-posterior knob  $\phi_1$  is sweeping over the whole workspace while left-right knob  $\phi_2$  is fixed one condition ( $0, \pm 30, \pm 60, \pm 90$  degrees). Change of dead zone with interpolation is demonstrated.

but this keep changed to  $0, \pm 30, \pm 60$ . We did this with and without compensator  $F$  to compare. (2) *Two DOF test*: Both  $\phi_1$  and  $\phi_2$  are simultaneously moving. We applied a sine wave with the range of the range of  $\pm 60$  degrees, But we applied different velocity;  $\phi_1$  works with  $60^\circ/\text{sec}$  while  $\phi_2$  works with  $120^\circ/\text{sec}$ . This leads the period of  $\phi_2$  is twice times period of  $\phi_1$ . All the data collection comes with EM tracking sensor to get the real measure.

##### B. Result of the non-linear hysteresis compensation

We tested three catheters, which has different hysteresis curve, but we modeled and identified parameters based on our proposed method. To evaluate the proposed method, we demonstrate the magnitude of the peak-to-peak, which is measured the highest value and the lowest value of the sine wave. In addition, we use the root mean squared error (RMSE) to show errors.

Due to the limited page, we show only one figure for 1 DOF out of four catheters in Figure 8. However, we show the overall performance evaluation in Table I-II. Table I shows the peak-to-peak error, which shows our proposed method improved the peak-to-peak error by 32 to 48 %. Table II shows a promising improvement by 45 to 57 %. Catheter 1 is shown in Figure 8; The first two row is for  $\phi_1$  motion while the last two row is for  $\phi_2$  motion. We shows time versus output angle and the input angle versus the output angle. From the second and fourth row of Figure 8, our proposed method compensates motions such that the blue-dot line is changed to the red-dot line, which is close to the linear line.

We demonstrate 2 DOF results for three catheters in Figure 9. The first two column is for catheter 1. The next two is for catheter 2, the last two is for catheter 3. The first row shows time versus output angle for  $\phi_1$  and  $\phi_2$  having different frequency. The second row shows the input angle versus the output angle for  $\phi_1$  and  $\phi_2$  motions. We also show the peak-to-peak error and RMSE in Table III. The results show that the peak-to-peak error is improved by 20.42%, and RMSE is improved by 48% over our test range.

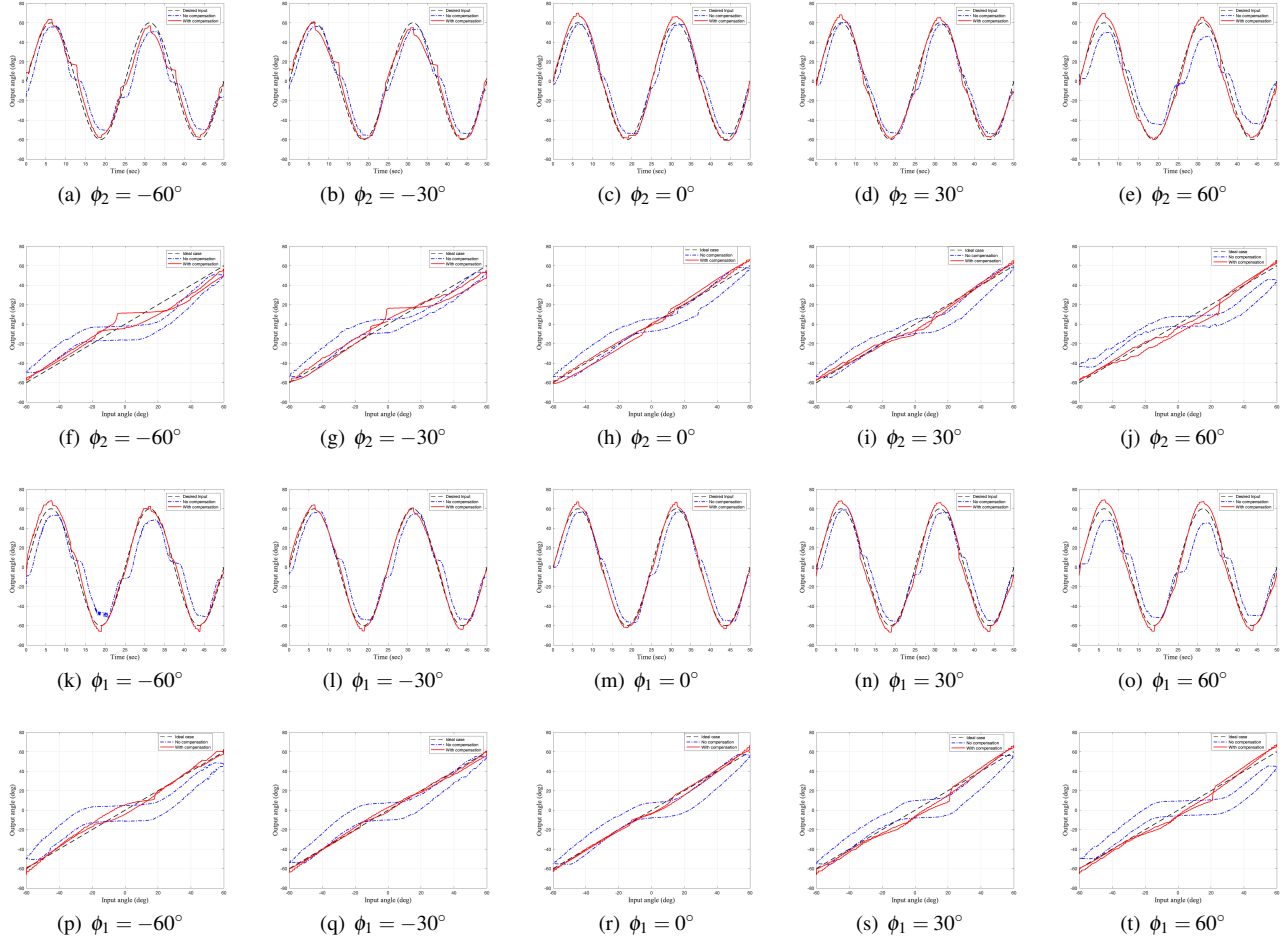


Fig. 8. The result of the non-linear behavior compensation for catheter 1: The black dot is the ground truth. The blue dot is without compensation. The red dot is with our compensation. The first row shows time versus output angle, and the second row shows the input angle versus the output angle for the anterior-posterior knob  $\phi_1$  motion, thus the left-right knob  $\phi_2$  is fixed as addressed. The third and the fourth rows are for the left-right knob  $\phi_2$  motion accordingly.

TABLE I  
PEAK-TO-PEAK ERRORS OF 1-DOF FOR ALL CATHETERS

Fixed angle from other DOF	$-60^\circ$	$-30^\circ$	$0^\circ$	$30^\circ$	$60^\circ$
No compensation (deg)	50.15	41.84	39.00	41.54	48.07
With compensation (deg)	33.89	27.22	20.16	25.66	27
Improvement rate (%)	32.42	34.94	48.29	38.21	43.84

TABLE III  
PEAK-TO-PEAK ERROR AND RMSE FOR 2-DOFs FOR ALL CATHETERS

Error	Peak-to-peak	RMSE
No compensation	44.48	14.76
With compensation	35.39	9.27
Improvement rate (%)	20.42	48.29

TABLE II  
ROOT MEAN SQUARED ERROR OF 1-DOF FOR ALL CATHETERS

Fixed angle from other DOF	$-60^\circ$	$-30^\circ$	$0^\circ$	$30^\circ$	$60^\circ$
No compensation (deg)	16.67	12.83	11.67	11.83	15.83
With compensation (deg)	9.16	6.5	5.33	6.33	6.67
Improvement rate (%)	45.00	49.35	54.29	46.48	57.89

The experimental results show that the proposed method is effective to compensate for non-linear hysteresis. Figures 8 shows typical examples; there is a delay in the dead zone before compensation, but it is reduced after compensation. In addition, the desired input angle 60 degree was not reached before compensation, but it can reach 60 degree. Lastly, the shape of the graph shows a straight line shape similar to the ideal case after compensation, which is shown in Figure 8 from (f) to (j), and from (p) to (t).

Our model is the piecewise linear approximation so there

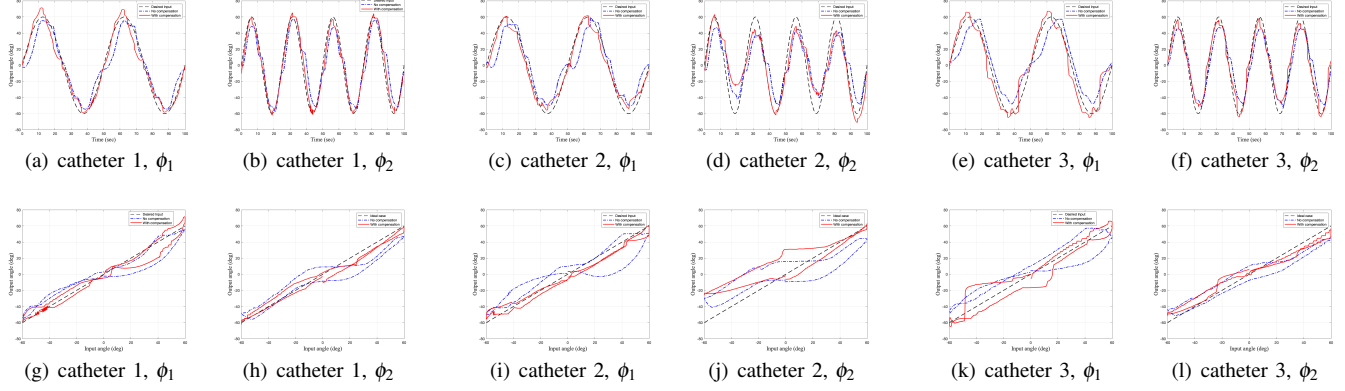


Fig. 9. This demonstrates 2 DOF results for three catheter: The black dot is the ground truth. The blue dot is without compensation. The red dot is with our compensation. The first two column is for catheter 1. The next one is for catheter 2, the last one is for catheter 3. The first row shows time versus output angle,  $\phi_1$  and  $\phi_2$  have different frequency as we designed. The second row shows the input angle versus the output angle for  $\phi_1$  and  $\phi_2$  motions.

exists a limitation, which might be able to show a jerk motion in transitions. For example, our approach generate the shape changes when entering or exiting the dead zone. However, we can observe that there is a discrepancy between real phenomena (Figure 3 and our model (Figure 5). Also the backlash hysteresis section is not straight line as we did in real phenomena. For this reason, we can observe the jerk movement.

The result of two DOF shows also good improvement, however, it is not as good as one DOF test. We believe that there exist a coupling effects in mechanical structures, which is not detected as much as we expected. However, most commercial products of TSM has a complicated mechanical structures inside due to considerations of multiple uses (e.g., ultrasound image, grasping tools). In our previous work [12], we demonstrated the method to compensate the plastic torsion effects due to coupling. However, it is also in constrained environments (the shape of sheath is linear). We think the motor current is limited to detect coupling effects, thus it might be necessary to add external sensors like load cells and tip tracking.

Our experimental setup has the shape constraints, which is the shape of the sheath in a straight line. First, we wanted to understand the relationship between motor current and hysteresis so that we can design methods to identify model parameters using motor current. We know that changes of the sheath shape is another challenging problem. However, based on our observation, shape changes mostly affect the width of dead zone  $D$ . Since we can detect  $D$  using motor current, if motions are allowed in working environments, we might be able to update parameters according to shapes.

## VI. CONCLUSION

In this paper, we proposed a simplified piece-wise linear model to compensate non-linear hysteresis of both dead zone and backlash in tendon-sheath-mechanism. Moreover, We proposed a simple parameter identification method for practical settings (e.g., surgical room) based on our validation

of relationship between hysteresis curve and motor current. Through the relationship between the non-linear hysteresis and the behavior of the motor current, the range of the dead zone  $D$  and the size of the backlash hysteresis  $B$  are obtained, and we get the slope of the straight line  $A$  through mechanical properties or data-driven method. Accordingly, the height of the dead zone  $H$  can be computed. All the parameters of our model were easily determined. Based on our proposed method, we can easily calibrate robotic manipulators for multiple medical devices without external sensors, which are not always possible in clinical environments. We applied our methods for ICE catheter robotic manipulators. We demonstrated 1-DOF and 2-DOF cases. The results show the errors for both are significantly reduced.

## DISCLAIMER

The concepts and information presented in this abstract/paper are based on research results that are not commercially available. Future availability cannot be guaranteed.

## REFERENCES

- [1] E. Daoud, S. Kalbfleisch, and J. Hummel, “Intracardiac echocardiography to guide transseptal left heart catheterization for radiofrequency catheter ablation,” *Journal of Cardiovascular Electrophysiology*, vol. 10, no. 3, pp. 358–363, 1999.
- [2] M. Khoshnam, I. Khalaji, and R. V. Patel, “A robotics-assisted catheter manipulation system for cardiac ablation with real-time force estimation,” in *2015 IEEE/RSJ International Conference on Intelligent Robots and Systems (IROS)*. IEEE, 2015, pp. 3202–3207.
- [3] M. Khoshnam and R. V. Patel, “Robotics-assisted control of steerable ablation catheters based on the analysis of tendon-sheath transmission mechanisms,” *IEEE/ASME Transactions on Mechatronics*, vol. 22, no. 3, pp. 1473–1484, 2017.
- [4] R. Bai, L. Di Biase, M. Valderrabano, F. Lorgat, H. Mlcochova, R. Tilz, U. Meyerfeldt, P. M. Hranitzky, O. Wazni, P. Kanagaratnam *et al.*, “Worldwide experience with the robotic navigation system in catheter ablation of atrial fibrillation: methodology, efficacy and safety,” *Journal of cardiovascular electrophysiology*, vol. 23, no. 8, pp. 820–826, 2012.
- [5] E. M. Khan, W. Frumkin, G. A. Ng, S. Neelagaru, F. M. Abi-Samra, J. Lee, M. Giudici, D. Gohn, R. A. Winkle, J. Sussman

*et al.*, “First experience with a novel robotic remote catheter system: Amigo™ mapping trial,” *Journal of Interventional Cardiac Electrophysiology*, vol. 37, no. 2, pp. 121–129, 2013.

[6] L. Ott, F. Nageotte, P. Zanne, and M. de Mathelin, “Robotic assistance to flexible endoscopy by physiological-motion tracking,” *IEEE Transactions on Robotics*, vol. 27, no. 2, pp. 346–359, 2011.

[7] H. M. Le, T. N. Do, and S. J. Phee, “A survey on actuators-driven surgical robots,” *Sensors and Actuators A: Physical*, vol. 247, pp. 323 – 354, 2016.

[8] P. Dario and C. A. Mosse, “Review of locomotion techniques for robotic colonoscopy,” in *2003 IEEE International Conference on Robotics and Automation (Cat. No.03CH37422)*, vol. 1, 2003, pp. 1086–1091 vol.1.

[9] S. J. Phee, W. S. Ng, I. M. Chen, F. Seow-Choen, and B. L. Davies, “Locomotion and steering aspects in automation of colonoscopy. i. a literature review,” *IEEE Engineering in Medicine and Biology Magazine*, vol. 16, no. 6, pp. 85–96, 1997.

[10] G. Chen, M. T. Redarce, and T. Redarce, “Development and kinematic analysis of a silicone-rubber bending tip for colonoscopy,” in *Proceedings of the International Conference on Intelligent Robots and Systems*, Beijing, China, Oct. 2006.

[11] P. M. Loschak, L. J. Brattain, and R. D. Howe, “Algorithms for automatically pointing ultrasound imaging catheters,” *IEEE Transactions on Robotics*, vol. 33, no. 1, pp. 81–91, Feb 2017.

[12] Y.-H. Kim, J. Collins, Z. Li, P. Chinnadurai, A. Kapoor, C. H. Lin, and T. Mansi, “Towards automatic manipulation of intracardiac echocardiography catheter,” 2020.

[13] M. Kaneko, T. Yamashita, and K. Tanie, “Basic considerations on transmission characteristics for tendon drive robots,” in *Fifth International Conference on Advanced Robotics 'Robots in Unstructured Environments*, 1991, pp. 827–832 vol.1.

[14] M. Kaneko, W. Paetsch, and H. Tolle, “Input-dependent stability of joint torque control of tendon-driven robot hands,” *IEEE Transactions on Industrial Electronics*, vol. 39, no. 2, pp. 96–104, 1992.

[15] L. S. Chiang, P. S. Jay, P. Valdastri, A. Menciassi, and P. Dario, “Tendon sheath analysis for estimation of distal end force and elongation,” in *2009 IEEE/ASME International Conference on Advanced Intelligent Mechatronics*, 2009, pp. 332–337.

[16] T. Fuxiang and W. Xingsong, “The design of a tendon-sheath-driven robot,” in *2008 15th International Conference on Mechatronics and Machine Vision in Practice*, 2008, pp. 280–284.

[17] L. Chen and X. Wang, “Modeling of the tendon-sheath actuation system,” in *2012 19th International Conference on Mechatronics and Machine Vision in Practice (M2VIP)*, 2012, pp. 489–494.

[18] G. Palli and C. Melchiorri, “Model and control of tendon-sheath transmission systems,” in *Proceedings 2006 IEEE International Conference on Robotics and Automation, 2006. ICRA 2006.*, 2006, pp. 988–993.

[19] G. Palli and C. Melchiorri, “Optimal control of tendon-sheath transmission systems,” *IFAC Proceedings Volumes*, vol. 39, no. 15, pp. 73 – 78, 2006.

[20] R. Zglimbea, V. Finca, E. Greaban, and M. Constantin, “Identification of systems with friction via distributions using the modified friction lugre model,” in *Proceedings of the 13th WSEAS International Conference on Systems*, ser. ICS’09, 2009, p. 579–584.

[21] V. Hassani and T. Tjahjowidodo, “Structural response investigation of a triangular-based piezoelectric drive mechanism to hysteresis effect of the piezoelectric actuator,” *Mechanical Systems and Signal Processing*, vol. 36, no. 1, pp. 210 – 223, 2013.

[22] T. Do, T. Tjahjowidodo, M. Lau, T. Yamamoto, and S. Phee, “Hysteresis modeling and position control of tendon-sheath mechanism in flexible endoscopic systems,” *Mechatronics*, vol. 24, no. 1, pp. 12 – 22, 2014.

[23] T. Do, T. Tjahjowidodo, M. Lau, and S. Phee, “Adaptive control for enhancing tracking performances of flexible tendon–sheath mechanism in natural orifice transluminal endoscopic surgery (notes),” *Mechatronics*, vol. 28, pp. 67 – 78, 2015.

[24] F. I. Mohammed Ismail and J. Rodellar, “The hysteresis bouc-wen model, a survey,” vol. 16, no. 2. Springer, 2009, pp. 161–188.

[25] P. Cabras, F. Nageotte, P. Zanne, and C. Doignon, “An adaptive and fully automatic method for estimating the 3d position of bendable instruments using endoscopic images,” *The International Journal of Medical Robotics and Computer Assisted Surgery*, vol. 13, no. 4, p. e1812, 2017.

[26] A. Reiter, P. K. Allen, and T. Zhao, “Appearance learning for 3d tracking of robotic surgical tools,” *The International Journal of Robotics Research*, vol. 33, no. 2, pp. 342–356, 2014.

[27] D. Baek, J. H. Seo, J. Kim, and D. S. Kwon, “Hysteresis compensator with learning-based hybrid joint angle estimation for flexible surgery robots,” *IEEE Robotics and Automation Letters*, vol. 5, no. 4, pp. 6837–6844, 2020.

[28] H. Yoon, J. Jeon, J. H. Chung, and B. Yi, “Error compensation for a 2 dof bendable endoscope mechanism,” in *2013 13th International Conference on Control, Automation and Systems (ICCAS 2013)*, 2013, pp. 862–865.

[29] L. A. Zhang, R. Khare, E. Wilson, S. X. Wang, C. A. Peters, and K. Cleary, “Robotic assistance for manipulating a flexible endoscope,” in *2014 IEEE International Conference on Robotics and Automation (ICRA)*, 2014, pp. 5380–5385.

[30] K. Xu and N. Simaan, “An investigation of the intrinsic force sensing capabilities of continuum robots,” *IEEE Transactions on Robotics*, vol. 24, no. 3, pp. 576–587, 2008.

[31] T. Do, T. Tjahjowidodo, M. Lau, and S. Phee, “An investigation of friction-based tendon sheath model appropriate for control purposes,” *Mechanical Systems and Signal Processing*, vol. 42, no. 1, pp. 97 – 114, 2014.

[32] T. Do, T. Tjahjowidodo, M. Lau, and S. Phee, “Real-time enhancement of tracking performances for cable-conduit mechanisms-driven flexible robots,” *Robotics and Computer-Integrated Manufacturing*, vol. 37, pp. 197 – 207, 2016.